Investigating the Cause of the Alkaline Transition of Phytocyanins†

Mark D. Harrison,‡ Sachiko Yanagisawa, and Christopher Dennison*

Institute for Cell and Molecular Biosciences, Medical School, University of Newcastle upon Tyne, Newcastle upon Tyne, NE2 4HH, U.K.

Received August 12, 2004; Revised Manuscript Received October 26, 2004

ABSTRACT: The phytocyanins are a family of plant cupredoxins that have been subdivided into the stellacyanins, plantacyanins, and uclacyanins. All of these proteins possess the typical type 1 His_2Cys equatorial ligand set at their mononuclear copper sites, but the stellacyanins have an axial Gln ligand in place of the weakly coordinated Met of the plantacyanins, uclacyanins, and most other cupredoxins. The stellacyanins exhibit altered visible, EPR, and paramagnetic ^1H NMR spectra at elevated pH values and also modified reduction potentials. This alkaline transition occurs with a pK_a of ∼10 [Dennison, C., Lawler, A. T. (2001) *Biochemistry 40*, 3158−3166]. In this study we demonstrate that the alkaline transition has a similar influence on the visible, EPR, and paramagnetic NMR spectra of cucumber basic protein (CBP), which is a plantacyanin. The mutation of the axial Gln95 ligand into a Met in umecyanin (UMC), the stellacyanin from horseradish roots, and the axial Met89 into a Gln in CBP have very limited, yet similar, influence on the pK_a for the alkaline transition as judged from alterations in visible spectra. The complete removal of the axial ligand in the Met89Val variant of CBP results in a slightly larger decrease in the pK_a for this effect, but similar spectral alterations are still observed at elevated pH. Thus, the axial Gln ligand is not the cause of the alkaline transition in Cu(II) stellacyanins, and alterations in the active site structures of the phytocyanins have a limited effect on this feature. The conserved Lys residue found adjacent to the axial ligand in the sequences of all phytocyanins, and implicated as the trigger for the alkaline transition, has been mutated to an Arg in UMC. The influence of increasing pH on the spectroscopic properties of Lys96Arg UMC is almost identical to those of the wild type protein, and thus, this residue is not responsible for the alkaline transition. However, a positively charged residue in this position seems to be important for the correct folding of UMC. Other possible triggers for the effects seen in the phytocyanins at elevated pH are discussed along with the relevance of the alkaline transition.

The influence of pH on the spectroscopic and redox properties of electron transfer (ET)[1] metalloproteins is well-recognized. Increased distance between the residue that protonates/deprotonates and the redox site leads to the attenuation of these effects (*1*). A well-studied pH-induced conformation change occurs in cytochrome *c*, and many studies (for example, see refs *2*−*5*) have focused on this alkaline transition. The effect is due to the axially coordinating Met being replaced by amino ligands from deprotonated Lys residues at elevated pH. However, there is still uncertainty about which ionizable group triggers this conformational transition (*5*). Interest in the alkaline transition of cytochrome *c* not only stems from the intriguing metalloprotein biochemistry, but also from the influence of this effect on physiological reactivity (*3*, *6*) and a potential involvement in protein folding and aggregation (*7*, *8*). Certain cupredoxins, which possess a mononuclear type 1 copper site, display altered spectroscopic properties [for the Cu(II) protein] above pH ∼9 (*9*−*19*), which has been described as an alkaline transition (*14*). The reduction potential is also influenced at high pH in the cupredoxins (*13*, *16*−*18*) and thus the alkaline transition may play a physiological role by tuning ET reactivity. The cause of the effects seen at alkaline pH in cupredoxins, which is currently not known, is the focus of this study.

The cupredoxins that exhibit an alkaline transition all belong to the phytocyanin subclass, which includes the stellacyanins, plantacyanins, and uclacyanins (*18*, *20*−*22*). The members of these three groups of phytocyanins differ in a number of ways, but alterations in the nature of the coordination site, which influences their spectroscopic properties, are most important for the present study. Cupredoxins possess a copper ion strongly coordinated by the thiolate sulfur of a Cys and the imidazole nitrogens of two His residues (*23*). The copper is displaced from the plane of these three equatorial ligands, usually in the direction of a weakly coordinated axial Met. The type 1 copper sites of stellacyanins are unusual in that they possess an axial Gln

† We thank BBSRC (Grant 13/B16498), Universities UK for an ORS award to S.Y., and Newcastle University for funding.

* Corresponding author. Telephone: +44 191 222 7127. Fax: +44 191 222 6929. E-mail: christopher.dennison@ncl.ac.uk.

‡ Current address: Centre for Molecular Biotechnology, School of Life Sciences, Queensland University of Technology, Brisbane, Queensland 4001, Australia.

[1] Abbreviations: ET, electron transfer; RST, stellacyanin from *R. vernicifera*; LMCT, ligand to metal charge transfer; EPR, electron paramagnetic resonance; ENDOR, electron nuclear double resonance; NMR, nuclear magnetic resonance; UMC, umecyanin, the stellacyanin from horseradish roots; MAV, mavicyanin, the stellacyanin from zucchini; BCB, a stellacyanin from *A. thaliana*; CBP, cucumber basic protein; WT, wild type; Hepes, 4-(2-hydroxyethyl)piperazine-1-ethanesulfonic acid; Caps, 3-[cyclohexylamino]-1-propanesulfonic acid; UV−vis, ultraviolet−visible; LF, ligand field.

10.1021/bi048256v CCC: $30.25
Published on Web 02/03/2005

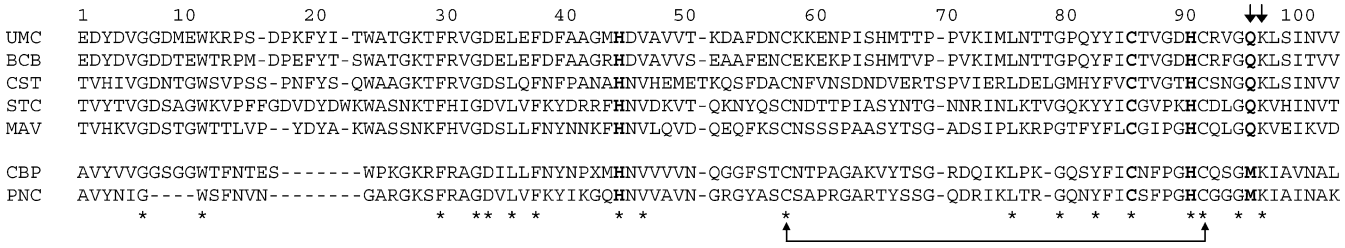

FIGURE 1: Multiple sequence alignment of the cupredoxin domains of selected phytocyanins generated using ClustalW (*28*). UMC; *Amoracia laphatifolia* (horseradish) stellacyanin (umecyanin) (*29*), BCB; *A. thaliana* stellacyanin (*30*), CST; *C. sativus* (cucumber) stellacyanin (*31*), STC; *R. vernicifera* (Japanese lacquer tree) stellacyanin (*32*), MAV; *Cucurbita pepo medullosa* (zucchini) stellacyanin (also called mavicyanin) (*33*), CBP; *C. sativus* plantacyanin (*34*); PNC, *Spinacia oleracea* (spinach) plantacyanin (*35*). Copper ligands are shown in bold and the residues mutated in this study are indicated by an arrow. Cys residues involved in the disulfide bond are linked by an arrow, while absolutely conserved residues are indicated with an asterisk.

ligand (*24*, *25*), whereas the plantacyanins (*26*, *27*) and uclacyanins have the more customary Met in this position (see Figure 1).

The first demonstration of the alkaline transition in a phytocyanin was published almost 40 years ago (*9*) for the stellacyanin (RST) from the Japanese lacquer tree (*Rhus vernicifera*). The effect was identified as it involves the Cu(II) protein changing from its characteristic blue color [due to a S(Cys)→Cu(II) ligand to metal charge transfer (LMCT) transition at ~600 nm (*36*)] at neutral pH to violet at higher pH (the LMCT band shifts to ~580 nm). The transition also influences the electron paramagnetic resonance (EPR), electron nuclear double resonance (ENDOR) (*37*), and paramagnetic ^{1}H nuclear magnetic resonance (NMR) (*14*, *18*) spectral properties of the protein and thus must alter the active site structure. A similar transition has been demonstrated in a number of other stellacyanins, including umecyanin (UMC, the stellacyanin from horseradish roots) (*10*, *17*), mavicyanin (MAV, the stellacyanin from zucchini) (*15*, *16*), BCB (a stellacyanin from *Arabidopsis thaliana*) (*19*), and certain plantacyanins (*11*, *12*), including the protein from *Cucumis sativus* (the plantacyanin from cucumber is commonly referred to as cucumber basic protein, CBP). A detailed investigation of the influence of the alkaline transition on the spectroscopic properties of CBP, or any other plantacyanin, has not been reported, and the effect has not been demonstrated in any member of the uclacyanin family.

A number of suggestions have been made for the cause of the alkaline transition in the phytocyanins. A particularly attractive proposal involves a change in the coordination mode of the axial Gln ligand in the stellacyanins from $O^{\epsilon 1}$ at neutral pH to $N^{\epsilon 2}H^-$ at more alkaline pH (*37*, *38*). However, given that the pK_a for the $N^{\epsilon 2}H_2$ moiety is very high (~15) and that paramagnetic NMR studies have demonstrated that the coordination mode of the axial Gln ligand is unaltered at elevated pH in the Ni(II) derivative of UMC (*25*), this seems unlikely. Almost all available phytocyanin sequences possess a Lys adjacent to the axial ligand (see Figure 1). Deprotonation of this residue has been suggested as the cause of the effect (*17*, *18*, *39*−*41*), although it is not thought that the Lys residue coordinates to the metal in the high pH form (as is cytochrome *c*). The involvement of this residue is supported by similar pH dependence of the spectroscopic properties of an azurin variant in which a Lys residue is introduced close to the active site (*42*). It has also been proposed that the phytocyanins are flexible molecules that undergo a change in secondary structure upon deprotonation of a surface residue that alters the coordination sphere of the copper (*14*, *21*). Herein we have investigated the cause of the alkaline transition using site-directed mutagenesis studies of the stellacyanin UMC and the plantacyanin CBP.

MATERIALS AND METHODS

Materials. Oligonucleotides were obtained from MWG Biotech AG. pET11a vector, *Escherichia coli* BL21(DE3) cells, and *E. coli* ORIGAMI B(DE3) cells were purchased from Novagen. Restriction enzymes were purchased from New England Biolabs, *Pfu* DNA polymerase and pGEM-T vector were obtained from Promega, and *Taq* DNA polymerase was purchased from Sigma. The sequences of both strands of all PCR products were determined.

Production of Mutants. Mutagenic primers (Table S1) were used with pMHCD1.4 as the template DNA (*19*) to convert Lys96 into Arg in UMC (using P1 and P2, thereby creating pMHCD1.6) via QuikChange (Stratagene) site-directed mutagenesis, according to the manufacturers protocols. *E. coli* BL21 (DE3) cells were transformed with pMHCD1.6 and the Lys96Arg variant of UMC, which is localized to the insoluble fraction (presumably as inclusion bodies), was obtained using a similar procedure as for wild type (WT) UMC (*19*). The Gln95Met UMC variant was produced as described elsewhere (*43*). Pure proteins with A_{280}/A_{606} ratios of 3.6 and yields of ~7 mg L^{-1} of culture were obtained.

An artificial coding region for the 96 amino acid residues of CBP (see Figure 1) has been synthesized using a method described previously (*19*) (the details of this will be reported elsewhere) and was cloned into pET11a, to create pETCBP. ORIGAMI B cells were transformed with pETCBP and protein overexpression and purification (which will be reported elsewhere) resulted in approximately 6 mg L^{-1} of culture of pure CBP with an A_{278}/A_{595} ratio of 6.0. Mutagenic primers were used to convert Met89 into Gln (P3 and P4; see Table S1 of the Supporting Information) and Val (P5 and P6; see Table S1) via QuikChange site-directed mutagenesis. The resulting constructs pETm89qCBP and pETm89vCBP were used to transform *E. coli* ORIGAMI B cells, and protein expression and purification were performed using the same procedure as for WT CBP. Met89Gln CBP with an A_{278}/A_{595} ratio of 5.0 gave a single band on a 15% SDS−PAGE gel and was produced with a yield of ~4 mg L^{-1} of culture. The Met89Val variant was produced in much lower amounts (~1 mg L^{-1} of culture) and protein with a A_{278}/A_{614} ratio of 4.0 gave a single band on a 15% SDS−PAGE gel.

Protein Samples for UV−Vis and Paramagnetic ^{1}H NMR Studies. For ultraviolet−visible (UV−vis) and paramagnetic NMR experiments, proteins were fully oxidized using a solution of $K_3[Fe(CN)_6]$. Excess oxidant was removed using an ultrafiltration cell (Amicon, 5 kDa cutoff membrane), and the proteins were usually exchanged into 10 mM potassium phosphate buffer. For the paramagnetic NMR experiments, samples were prepared in 99.9% D_2O and 90% H_2O/10% D_2O and typically contained 3−4 mM protein. The pH of protein solutions were measured using a narrow pH probe (Russell KCMAW11) with an Orion 420A pH meter. The pH of the sample was adjusted using NaOD or DCl in deuterated solutions and NaOH and HCl in H_2O solutions.

UV−Vis Spectrophotometry. UV−vis spectra were acquired at 25 °C on a Perkin-Elmer λ35 spectrophotometer. The molar extinction coefficients of the proteins were determined as described elsewhere (*19*).

EPR Spectroscopy. X-band EPR spectra were recorded on a Bruker EMX spectrometer at −196 °C, and 2,2-diphenyl-1-picrylhydrazyl was used as the reference. Samples typically contained 1−2 mM protein in 40% glycerol and 25 mM 4-(2-hydroxyethyl)piperazine-1-ethanesulfonic acid (Hepes) at pH 7.6 or 8.0 and also in 40 mM 3-[cyclohexylamino]-1-propanesulfonic acid (Caps) plus 10% glycerol at pH ∼11. The spectra were simulated using the program SimFonia (Bruker).

NMR Spectroscopy. Paramagnetic ^{1}H NMR spectra were acquired on a JEOL Lambda 500 spectrometer usually at 25 °C as described previously (*25*).

RESULTS

UV−Vis, EPR, and Paramagnetic NMR Spectra of Cu(II) UMC Variants. The UV−vis spectra of Gln95Met and Lys96Arg UMC at pH 7.6 are presented in Figure 2, parts A and B, respectively, and the positions and intensities of bands are listed in Table 1, along with those for the WT protein. The UV−vis spectrum of the Lys96Arg variant closely resembles that of WT UMC, with only slight differences in the intensities of the two LMCT bands [the band at ∼450 nm in the spectra is also due to a S(Cys)→Cu(II) LMCT transition (*36*)], whereas replacement of the axial Gln ligand with a Met has a more significant effect (Table 1). The X-band EPR spectra of Gln95Met, Lys96Arg, and WT UMC are shown in Figure S1 of the Supporting Information, along with the parameters obtained from simulations. The spectra of Lys96Arg and WT UMC are very similar, whereas in the spectrum of the Gln95Met variant a significant decrease in g_z, an increase in A_z, and a slightly larger separation between g_x and g_y are observed. All of the spectroscopic features of Gln95Met UMC are consistent with the replacement of the Gln ligand with a weak axially coordinating Met (*43*). The paramagnetic ^{1}H NMR spectrum of Lys96Arg UMC is very similar to that of the WT protein (see Figure S2 and Table S2) consistent with this mutation having very little influence on the active site structure. We have assigned the paramagnetic ^{1}H NMR spectrum of Gln95Met UMC previously (*43*) and the additional broad resonance at ∼25 ppm arises from one of the C$^\gamma$H protons of the introduced axial Met95 ligand (see Figure S2 and Table S2).

Spectroscopic Properties of Cu(II) WT CBP and the Met89Gln and Met89Val Variants. The UV−vis spectra of WT, Met89Gln, and Met89Val CBP at around neutral pH are presented in Figure 3, parts A, B, and C, respectively, with the positions and intensities of bands listed in Table 1. The altered intensities of the LMCT bands in the UV−vis spectrum and the influence of the Met89Gln mutation on the EPR spectrum of CBP (data not shown) are the reverse of what is observed upon making the Gln95Met mutation in UMC and are consistent with the replacement of the weakly coordinated thioether sulfur of Met89 with the O$^{\epsilon 1}$ of Gln89 as the axial ligand. The Met89Val CBP variant possesses a decreased A_z value in its EPR spectrum (data not shown) and an increase in the energy of the ligand field (LF) transitions in its UV−vis spectrum consistent with the absence of an axial ligand (*44*). The Asn40 C$^\alpha$H resonance is readily assigned in the paramagnetic NMR spectra of WT and Met89Gln CBP as is one of the axial Met89 C$^\gamma$H resonances in the spectrum of the WT protein (data not shown). Resonances from the axial Gln ligand are not observed in the spectrum of Met89Gln CBP, which is consistent with paramagnetic NMR studies of UMC (see Figure S2) and other stellacyanins (*14*, *17*−*19*, *25*, *45*).

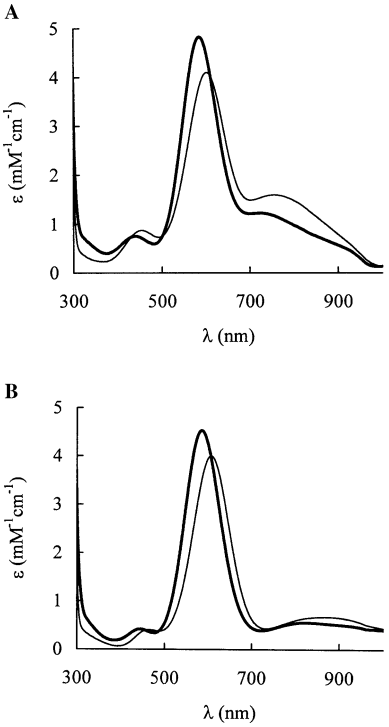

FIGURE 2: UV−vis spectra (25 °C) of oxidized proteins in 10 mM potassium phosphate buffer: (A) Gln95Met UMC at pH 7.6 (thin line) and at pH 10.5 (thicker line), (B) Lys96Arg UMC at pH 7.6 (thin line) and at pH 10.8 (thicker line).

The Alkaline Transition. Increasing pH (above ∼9) has a dramatic effect on the spectroscopic properties of the phytocyanins (*9*−*19*). The sizable influence of the alkaline transition on the EPR spectrum of Cu(II) CBP is shown in Figure 4 and on the paramagnetic NMR spectrum of Ni(II) UMC is shown in Figure 5 [more resonances are directly observed in the paramagnetic NMR spectrum of the Ni(II) derivative than Cu(II) UMC (*17*, *25*), allowing a more detailed analysis of the influence of the alkaline transition]. The alkaline transition also has a significant effect on the UV−vis spectra of phytocyanins (see Figures 2 and 3). In this study, the influence of selected mutations on the alkaline transition in UMC and CBP has been assessed by analyzing

Table 1: Properties of the Cu(II) Forms of WT, Lys96Arg, and Gln95Met UMC and WT and Met89Gln CBP[a]

	UMC			CBP	
parameter	WT[b]	Gln95Met	Lys96Arg	WT	Met89Gln
λ_1[c] (nm) [ϵ_1 (M^{-1} cm^{-1})] pH ~8[d]	606 [4300]	601 [4100]	606 [4000]	595 [3200]	595 [4100]
λ_1 (nm) [ϵ_1 (M^{-1} cm^{-1})] pH ~11[e]	584 [4310]	585 [4820]	585 [4530]	584 [3770]	576 [4480]
pK_a λ_1	9.7	9.3	9.8	9.7	9.5
λ_2[c] (nm) [ϵ_2 (M^{-1} cm^{-1})] pH ~8[d]	464 [500]	453 [870]	464 [400]	442 [1800]	447 [1170]
λ_2 (nm) [ϵ_2 (M^{-1} cm^{-1})] pH ~11[e]	443 [470]	439 [750]	443 [420]	432 [1630]	432 [1090]
pK_a λ_2	9.7	9.5	10.0	9.9	9.6
ϵ_2/ϵ_1 (pH ~ 8)[d]	0.12	0.21	0.10	0.56	0.29
ϵ_2/ϵ_1 (pH ~ 11)[e]	0.11	0.16	0.09	0.43	0.24
δ (ppm) Asp45/Asn40[f] $C^{\alpha}H$ (pH ~8)[g]	13.7	16.0	14.0	16.7	16.5
δ (ppm) Asp45/Asn40[f] $C^{\alpha}H$ (pH ~11)[h]	12.8	14.1	13.0	15.1	14.9
EPR spectral properties	axial	axial	axial	rhombic	rhombic

[a] In the case of Met89Val CBP, λ_1 occurs at 614 nm (ϵ_1 = 5000 M^{-1} cm^{-1}) at pH 7.8 and shifts to 595 nm (ϵ_1 = 5050 M^{-1} cm^{-1}) at pH 9.6, giving a pK_a λ_1 of 8.9. [b] As reported in ref *19*. [c] The bands at ~600 and ~450 nm in the UV−vis spectra of cupredoxins are due to S(Cys)→Cu(II) LMCT transitions. [d] pH 7.6 for WT, Lys96Arg, and Gln95Met UMC, pH 8.0 for WT CBP, and pH 7.8 for Met89Gln CBP. [e] pH 10.8 for WT and Lys96Arg UMC, pH 10.5 for Gln95Met UMC, pH 10.6 for WT CBP, and pH 11.0 for Met89Gln CBP. [f] Asp45 in WT and UMC variants and Asn40 in WT and Met89Gln CBP. [g] pH 7.6 for WT, Lys96Arg, and Gln95Met UMC (all at 40 °C) and pH 8.0 for WT and Met89Gln CBP (both at 25 °C). [h] pH 10.5 for WT and Lys96Arg UMC, pH 10.4 for Gln95Met UMC (all at 40 °C), pH 10.6 for WT CBP, and pH 10.5 for Met89Gln CBP (both at 25 °C).

mainly their UV−vis spectra. In particular, the roles of the axial ligand and the adjacent conserved Lys residue, which have both been associated with the alkaline transition, have been studied by site-directed mutagenesis. Approximately 20 nm shifts to lower wavelength are observed for both LMCT bands upon increasing pH in the proteins studied. In all cases this process is completely reversible, and isosbestic points are observed, indicating the presence of two-state pH-dependent equilibria.

In the UV−vis spectrum of Gln95Met UMC, the band at 601 nm at neutral pH shifts to 585 nm and increases in intensity, when the pH is raised to 10.5 (see Figure 2A and Table 1). The dependence of the position of this visible absorption band upon pH (see Figure 6A) can be fit (three parameters, nonlinear least squares) to eq 1 corresponding to a two-state pH-dependent equilibrium

$$\lambda = (K_a\lambda_H + [H^+]\lambda_L)/(K_a + [H^+]) \quad (1)$$

where λ_H and λ_L are the wavelengths of the visible absorption band at high and low pH, respectively, yielding a pK_a of 9.3. The pH-dependence of the position of the second LMCT band (see Figure 2A and Table 1) gives a pK_a of 9.5. The intensities of these two bands are affected by the alkaline transition, and the $\epsilon_{439}/\epsilon_{585}$ ratio at pH 10.5 (0.16) is lower than the $\epsilon_{453}/\epsilon_{601}$ ratio at pH 7.6 (0.21). The LF bands between 700 and 900 nm shift to lower wavelength and decrease in intensity when the pH is increased as is also the case in WT UMC (*19*).

The main LMCT band in the UV−vis spectrum of Lys96Arg UMC shifts from 606 nm at neutral pH to 585 nm and increases in intensity, when the pH is increased to 10.8 (see Figure 2B). Figure 6A shows the pH-dependence of the position of this visible absorption band, and a fit of these data to eq 1 yields a pK_a of 9.8. The position of the second LMCT band is also pH-dependent (see Figure 2B and Table 1), giving a pK_a of 10.0. The intensities of these two bands are affected by the alkaline transition, but the $\epsilon_{464}/\epsilon_{606}$ ratio at pH 7.6 (0.10) is very similar to the $\epsilon_{443}/\epsilon_{585}$ ratio at pH 10.8 (0.09). The LF bands between 700 and 900 nm in the spectrum of Lys96Arg UMC also shift to lower wavelength and decrease in intensity when the pH is increased.

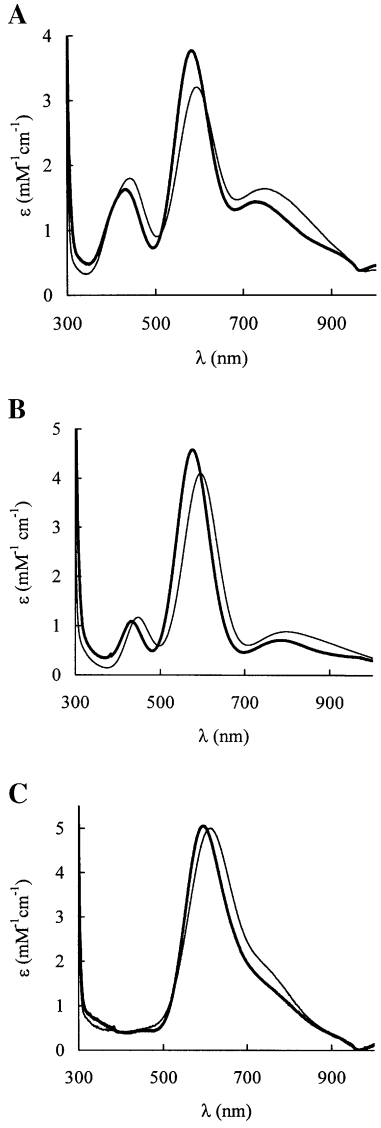

FIGURE 3: UV−vis spectra (25 °C) of oxidized proteins in 10 mM potassium phosphate buffer: (A) WT CBP at pH 8.0 (thin line) and at pH 10.6 (thicker line), (B) Met89Gln CBP at pH 7.8 (thin line) and at pH 11.0 (thicker line), and (C) Met89Val CBP at pH 7.8 (thin line) and at pH 9.6 (thicker line).

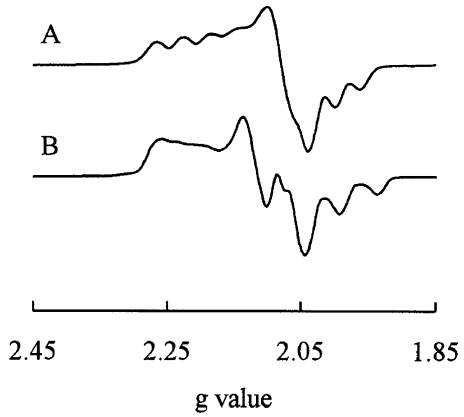

FIGURE 4: X-band EPR spectra of Cu(II) CBP at −196 °C. Spectrum A was obtained in 25 mM Hepes, pH 7.6 (40% glycerol), while spectrum B was obtained in 40 mM Caps (10% glycerol), pH 11.1. Parameters obtained from simulations (SimFonia) are $g_x = 2.018$, $A_x = 6.7$ mT, $g_y = 2.086$, $A_y = 0.5$ mT, $g_z = 2.205$, $A_z = 5.6$ mT for spectrum A and $g_x = 2.018$, $A_x = 9.6$ mT, $g_y = 2.068$, $A_y = 2.5$ mT, $g_z = 2.228$, $A_z = 3.4$ mT for spectrum B.

The UV−vis spectrum of WT CBP has a much more intense LMCT band at ∼450 nm than UMC (see Figure 3A). Nevertheless, the spectrum of CBP exhibits a similar dependence on pH with the LMCT bands shifting to lower wavelength upon increasing pH (Figure 3A and Table 1), giving pK_a values of 9.7 and 9.9 (see Figure 6B). It is apparent from Figure 6B that a second effect influences the UV−vis spectrum of WT CBP at pH ∼11 and higher, which is accompanied by irreversible color loss and precipitation of the protein [similar behavior has been reported for STC (*9*) and UMC (*10*)], and thus, data up to pH 10.6 only were used for analysis. The increase in the strength of the main LMCT band along with the decrease in the intensity of the peak at ∼440 nm results in the $\epsilon_{442}/\epsilon_{595}$ ratio of 0.56 at pH 8.0, falling to a $\epsilon_{432}/\epsilon_{584}$ ratio of 0.43 at pH 10.6. Interestingly, the LF bands in the 700−900 nm region of the UV−vis spectrum also shift to higher energy upon increasing pH in CBP, as is the case in UMC.

In the spectrum of Met89Gln CBP, the relative intensity of the two LMCT bands (at approximately neutral pH) is altered compared to the WT protein resulting in a $\epsilon_{447}/\epsilon_{595}$ ratio of 0.29 (see Figure 3B and Table 1). The positions and intensities of these two bands change in a similar manner as observed in the WT protein upon increasing pH (see Figures 3B and 6B and Table 1), giving pK_a values of 9.5 and 9.6 and a $\epsilon_{432}/\epsilon_{576}$ ratio of 0.24 at pH 11.0. The LF bands also shift to lower wavelength upon increasing pH in this CBP variant. In the UV−vis spectrum of Met89Val CBP, the main LMCT band is found at 614 nm at pH 7.8 with the band at around 450 nm possessing very little intensity (see Figure 3C). The 614 nm band shifts to lower wavelength upon increasing pH and is found at 595 nm at pH 9.6 (see Figures 3C and 6B), giving a pK_a of 8.9 (using data only up to pH 9.9). The pH-dependence of the positions of the second LMCT band and the LF transitions are difficult to follow in Met89Val CBP. The effect seen under very alkaline conditions (pH >10.5) in WT CBP also influences the UV−vis spectrum of the Met89Gln and in particular the Met89Val variant where onset occurs at pH 10.

The influence of the mutations made on the active site alterations caused by the alkaline transition has been assessed by analyzing the paramagnetic ^{1}H NMR spectra of the Cu(II) proteins. In all cases the alkaline transition results in a significant decrease (>1 ppm) in the chemical shift of the $C^{\alpha}H$ proton of the residue adjacent to the N-terminal His ligand (Asp45 in UMC and Asn40 in CBP). In WT CBP and the Gln95Met UMC variant, this is accompanied by 2 and 4 ppm decreases in the chemical shift of the Met89 and Met95 $C^{\gamma}H$ proton resonances, respectively. Signals arising from the axial ligand are not observed in the spectra of the proteins studied herein with a Gln in this position, and thus, no information about the influence of the alkaline transition on the interaction of this ligand with Cu(II) is obtained [in the spectra of Ni(II) UMC (see Figure 5) there is a decrease in the chemical shift values of the $C^{\gamma}H$ protons of the axial Gln95 ligand (*25*)]. The observed shifts of the imidazole ring resonances from the two His ligands are influenced by the alkaline transition in all of the proteins studied, but the very broad nature of these signals makes quantitative analysis difficult.

DISCUSSION

WT UMC and CBP have different active site structures and exhibit distinct spectroscopic properties. Both proteins possess the typical His_2Cys equatorial ligand set seen in all cupredoxins (*23*). However, in UMC the almost tetrahedral active site geometry is completed by a Gln ligand, which coordinates via its side chain amide oxygen atom [Cu(II)−$O^{\epsilon 1}$(Gln95) bond length of 2.26 Å] (*46*), whereas in CBP the trigonal pyramidal cupric site structure involves a weak axial Met ligand [Cu(II)−S^{δ}(Met89) bond length of 2.61 Å] (*26*). The axial EPR spectrum of UMC along with the low intensity of the LMCT band at ∼450 nm in its UV−vis spectrum results in this protein having a classic type 1 copper site (*36*). The EPR spectrum of CBP is rhombic and there is enhanced absorbance at ∼450 nm in its UV−vis spectrum, and thus this cupredoxin possesses a distorted (or perturbed) type 1 copper center (*36*). Regardless of these differences, the alkaline transition has a very similar influence on the UV−vis spectra of UMC and CBP (see Table 1) and occurs with identical pK_a values (9.7). The alkaline transition has a similar effect in other stellacyanins and occurs with pK_a values of 10.1, 9.7, and 9.0 in oxidized STC (*18*), BCB (*19*), and MAV (*16*), respectively. The likeness of the influence of the alkaline transition on the active site structure of UMC (and other stellacyanins) and CBP is confirmed by analogous alterations in the paramagnetic NMR spectra upon increasing pH (see Table 1). Thus, the different active site structures and spectroscopic properties (these two features are not inextricably linked, as many stellacyanins have distorted type 1 sites, whereas UMC has a classic center) observed in these two proteins do not influence the alkaline transition or its effect on the active site structure. Paramagnetic NMR studies demonstrate that the alkaline transition influences all of the coordinating residues with the M(II)−S(Cys) interaction most affected (for example, see Figure 5 and refs *14*, *17*, *19*, and *25*). This is consistent with the significant shifts of the S(Cys)→Cu(II) LMCT bands seen in the UV−vis spectra. The M(II)−S(Cys) interaction decreases at elevated pH (*14*, *17*−*19*, *25*), and there is a change in the conformation of this ligand (see Figure 5). The Cu(II)−S(Cys) bond is influenced in all of the proteins studied herein as the isotropic shift of the $C^{\alpha}H$ proton resonance of the residue adjacent to the N-terminal His ligand, which exhibits a sizable Fermi-

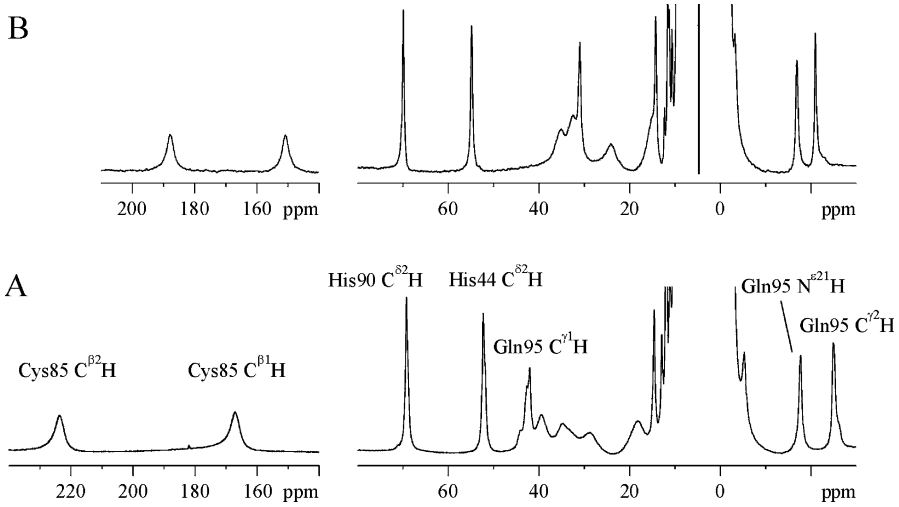

FIGURE 5: ^{1}H NMR spectra (300 MHz) of Ni(II) UMC at 30 °C in 90% H_2O/10% D_2O. The spectrum shown in part A was obtained at pH 8.0, while that in part B was collected at pH 10.7. Some of the assignments that have been made (*25*) are included in part A.

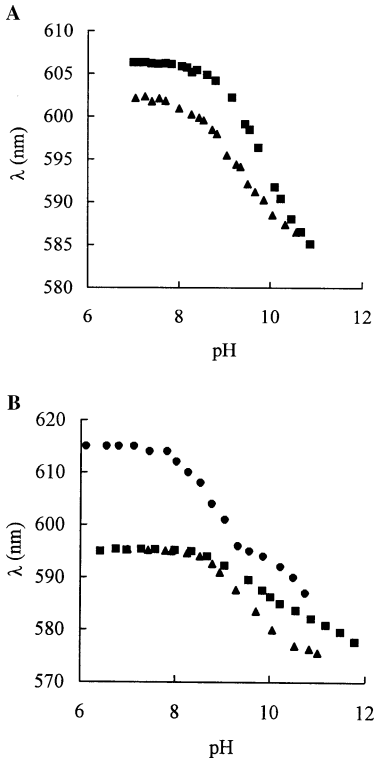

FIGURE 6: Dependence on pH (25 °C) of the position of the main visible absorption band of oxidized (A) Gln95Met (▲) and Lys96Arg (■) UMC and (B) WT (■), Met89Gln (▲), and Met89Val (●) CBP in 10 mM phosphate buffer.

contact contribution (*45*) due to its amide group hydrogen-bonding to the thiolate sulfur of the Cys ligand, decreases at elevated pH. The interaction with the axial ligand is also lowered by the alkaline transition (see Figure 5 and refs *14* and *25*), which is in agreement with the increased equatorial LF strength (*44*) and the decreased ϵ_2/ϵ_1 ratios (*36*) observed in all of the proteins studied upon increasing pH, and the decreased isotropic shifts of the $C^{\gamma}H$ proton resonances of the axial Met ligands in WT CBP and Gln95Met UMC. Thus the alkaline transition has a similar influence on the active site structure of all of the proteins studied.

Given the proposed role of the axial Gln ligand in the alkaline transition of stellacyanins, the influence of mutating this residue has been investigated. The Gln95Met UMC and Met89Gln CBP variants have altered spectroscopic properties compared to their respective WT proteins, which are consistent with the changes in axial ligand. The influence of increasing pH on the spectroscopic properties of these two variants is very similar to that observed in the WT proteins. Studies on Ni(II) UMC (see Figure 5) show that in this substituted stellacyanin the axial Gln ligand coordinates via its $O^{\epsilon 1}$ atom at alkaline pH (*25*). However, Cu(II) is more effective at promoting amide deprotonation (required for $N^{\epsilon 2}H^-$ coordination) than Ni(II) (*47*, *48*). Therefore, the observation of an alkaline transition in Gln95Met UMC (and also CBP) demonstrates that this effect does not involve an alteration in the coordination mode of the axial Gln in the Cu(II) stellacyanins. The fact that the introduction of an axial Gln in CBP also hardly alters the alkaline transition in this protein indicates that this effect is not influenced by variations in the active site structures in the phytocyanins. This is confirmed by the presence of the alkaline transition in the Met89Val CBP variant that does not possess an axial ligand. In Gln95Met UMC and the Met89Gln and Met89Val CBP variants, the pK_a for the alkaline transition decreases compared to the WT proteins with the largest influence caused by the Met89Val mutation to CBP. It is a little difficult to rationalize these decreases, but they are likely due to changes in the protein/active site structure as a result of the mutations made.

To investigate the possible role of the conserved Lys residue found adjacent to the axial ligand in all phytocyanins as a trigger for the alkaline transition (see Figures 1 and 7), we have characterized the Lys96Arg UMC variant. We also prepared the Lys96Met and Lys96Glu UMC variants, but these did not yield folded proteins with type 1 copper sites. However, the Lys96Arg variant did fold correctly and has a copper site with spectroscopic properties almost identical to those of the WT protein (the Lys96Arg mutation also has only a limited effect on the reduction potential of UMC; data not shown). The Lys96Arg mutation hardy influences the alterations of the spectral properties of UMC at elevated pH, and the pK_a value for the alkaline transition is unaffected. Lys96 is exposed on the surface of UMC (*46*), as is the corresponding Lys in all other structurally characterized phytocyanins (*24*, *26*, *27*), and this is anticipated to be the

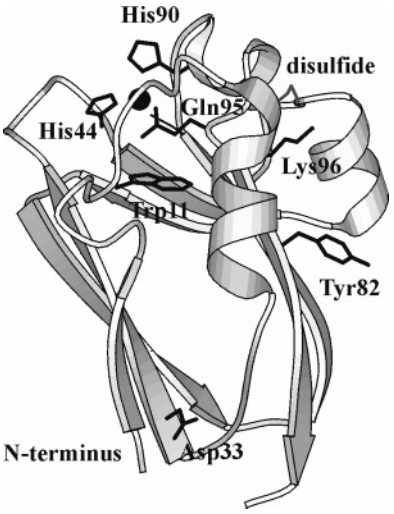

FIGURE 7: Structure of UMC (*46*) drawn with MOLSCRIPT (*49*) in which the Cu(II) ion is shown in black and the side chains of the coordinating amino acids are included. The residues that are most relevant to the present study are indicated, as is the disulfide bridge close to the active site.

case for Arg96 in the UMC variant. The typical pK_a value for a surface Lys residue is ~10.5 (*50*), while that for a surface Arg is above 12.0 (*50*). It is difficult to imagine that the microenvironment of residue 96 in UMC is such that amino and guanido groups in this position have identical pK_a values. Therefore, the lack of influence of the Lys96Arg mutation on the pK_a for the alkaline transition indicates that the conserved Lys adjacent to the axial ligand is not responsible for this effect in the phytocyanins. However, the presence of a basic residue next to the axial ligand appears to be essential for the refolding of WT UMC in vitro and may play an important role for the in vivo folding of all phytocyanins.

The question then remains as to the cause of the alkaline transition in the phytocyanins. It has been suggested that this subfamily of the cupredoxins are flexible molecules that change secondary structure at elevated pH (*14*, *21*). We have recently shown the structures of Cu(II) and Cu(I) UMC to be almost identical, indicating that this phytocyanin is reasonably rigid (*46*), and thus, overall flexibility is probably not a contributing factor to the alkaline transition. A number of ionizable residues are conserved in the amino acid sequences presented in Figure 1, and their positions in the structure of Cu(II) UMC (*46*) are indicated in Figure 7. The residue Trp11, which is involved in a π-amide interaction with the axial Gln95 ligand, could be responsible for the alkaline transition, but the pK_a of the Trp side chain is ~17 (*51*) which makes this unlikely. The conserved Asp33 is >23 Å from the copper ion, and the pK_a value must be too low for it to be implicated in the alkaline transition. Tyr82 is another potential trigger of the effects seen at elevated pH in the phytocyanins, but this residue is some 20 Å from the active site. Furthermore, all tyrosines have previously been shown to have pK_a values above 11 in both UMC (*10*) and CBP (*52*), thus making this residue type unlikely as the cause of the alkaline transition in the phytocyanins. Another ionizable species that possesses a pK_a in the correct range for the alkaline transition is the N-terminus. However, this group is always a long way from the copper site in the phytocyanins (*24*, *26*, *27*, *46*) and thus should not influence the active site. Furthermore, in WT UMC the N-terminus possesses an additional residue (Met0) introduced during cloning that does not alter the pK_a for the alkaline transition (*17*, *19*). The $N^{\epsilon 2}H$ moieties of the two His ligands are another possible cause of the alkaline transition in the phytocyanins (in all cupredoxins the His ligands coordinate via their $N^{\delta 1}$ atoms). The pK_a for the formation of an imidazolate is usually high (*53*), but coordination of the His to a metal ion can lower this. In rusticyanin (a cupredoxin), active site alterations that occur at alkaline pH (pK_a ~ 9) and result in the main LMCT band in the UV−vis spectrum shifting from 597 to 578 nm (and increasing in intensity) as the pH is increased (*54*) have been associated (*55*) with the deprotonation of the $N^{\epsilon 2}H$ of the exposed His143 ligand [originally a Lys or Tyr was thought to be responsible (*54*)]. The His ligands of the Rieske iron−sulfur center are also known to deprotonate at elevated pH (*53*). The deprotonation of a coordinated His at a redox center has a dramatic influence on the reduction potential (*53*, *54*), which is not the case in UMC (*17*) and STC (*18*) [however, the alkaline transition in MAV has a much larger effect on the reduction potential (*16*)], but this may be a consequence of the exposed nature (*24*, *26*, *27*, *46*) of the copper sites in the phytocyanins. It is interesting to note that the deprotonation of a coordinated His would strengthen its bond with Cu(II), which is consistent with the observed weakening of the Cu(II)−S(Cys) interaction at alkaline pH in the phytocyanins. In conclusion, it appears that the cause of the alkaline transition is not one of the more obvious candidate residues and may be due to a group or residue that displays uncharacteristic ionization properties.

The physiological relevance of the alkaline transition in cytochrome *c* has been described (*3*, *5*, *6*). The association of this redox metalloprotein with cytochrome *c* oxidase leads to changes similar to those observed at elevated pH that influence the reduction potential. Thus, the effects that are seen in vitro on isolated cytochrome *c* could play an important role in controlling the ET reactivity with physiological partners in vivo. The pH-induced changes observed in rusticyanin are reproduced by complexation with an ET partner, and thus, these alterations could also have a physiological role (*55*, *56*). A similar significance could apply to the alkaline transition in the phytocyanins, which also influences the reduction potential (*16*−*18*), although for these proteins the exact physiological function, and their redox protein partners, are currently unknown. Nevertheless, the association with a partner could induce similar changes to those observed at alkaline pH, altering the reduction potential and facilitating ET. It is important to note that ET between rusticyanin and its partner would be thermodynamically unfavorable without the shift in reduction potential observed upon complexation (*55*). This role of the exposed His ligand in regulating physiological reactivity is analogous to that suggested for the same ligand in the cupredoxins where protonation and dissociation from the Cu(I) site is observed at usually acidic pH (*57*). The alkaline form of CBP (see Figure 4B) and other phytocyanins (*9*, *10*, *17*) is unstable at higher pH. Furthermore, the introduction of a nonpositively charged residue at position 96 in UMC results in proteins that cannot refold from inclusion bodies (WT and Gln95Met UMC both readily refold). Although this residue does not trigger the observed active site alterations at alkaline pH,

the deprotonation of Lys96 destabilizes the protein. Thus, the effects seen at alkaline pH in the phytocyanins could be relevant to the formation of aggregates and also for protein folding intermediates, as suggested in cytochrome *c* (*7*, *8*).

SUPPORTING INFORMATION AVAILABLE

Tables showing the sequences of primers used for mutagenesis studies and listing the assignment of resonances in the paramagnetic ^{1}H NMR spectra of WT, Gln95Met, and Lys96Arg UMC and figures showing the EPR and paramagnetic ^{1}H NMR spectra of WT, Gln95Met, and Lys96Arg UMC. This material is available free of charge via the Internet at http://pubs.acs.org.

REFERENCES

1. Bashford, D., Karplus, M., and Canters, G. W. (1988) Electrostatic effects of charge perturbations introduced by metal oxidation in proteins. A theoretical analysis, *J. Mol. Biol. 203*, 507−510.
2. Ferrer, J. C., Guillemette, J. G., Bogumil, R., Inglis, S. C., Smith, M., and Mauk, A. G. (1993) Identification of Lys79 as an iron ligand in one form of alkaline yeast iso-1-ferricytochrome *c*, *J. Am. Chem. Soc. 115*, 7507−7508.
3. Rosell, F. I., Ferrer, J. C., and Mauk, A. G. (1998) Proton-linked protein conformational switching: Definition of the alkaline conformational transition of yeast iso-1-ferricytochrome *c*, *J. Am. Chem. Soc. 120*, 11234−11245.
4. Assfalg, M., Bertini, I., Dolfi, A., Turano, P., Mauk, A. G., Rosell, F. I., and Gray, H. B. (2003) Structural model for an alkaline form of ferricytochrome *c*, *J. Am. Chem. Soc. 125*, 2913−2922.
5. Martinez, R. E., and Bowler, B. E. (2004) Proton-mediated dynamics of the alkaline conformational transition of yeast iso-1-cytochrome *c*, *J. Am. Chem. Soc. 126*, 6751−6758.
6. Döpner, S., Hildebrandt, P., Rosell, F. I., Mauk, A. G., von Walter, M., Buse, G., and Soulimane, T. (1999) The structural and functional role of lysine residues in the binding domain of cytochrome *c* in the electron transfer to cytochrome *c* oxidase, *Eur. J. Biochem. 261*, 379−391.
7. Nelson, C. J., and Bowler, B. E. (2000) pH dependence of formation of a partially unfolded state of a Lys73 → His variant of iso-1-cytochrome *c*: Implications for the alkaline conformational transition of cytochrome *c*, *Biochemistry 39*, 13584−13594.
8. Hoang, L., Maity, H., Krishna, M. M. G., Lin, Y., and Englander, S. W. (2003) Folding units govern the cytochrome *c* alkaline transition, *J. Mol. Biol. 331*, 37−43.
9. Peisach, J., Levine, W. G., and Blumberg, W. E. (1967) Structural properties of stellacyanin, a copper mucoprotein from *Rhus vernicifera*, the Japanese Lac tree, *J. Biol. Chem. 242*, 2847−2858.
10. Sjöholm, I., and Stigbrand, T. (1974) Circular dichroism studies of the copper ligand structure of umecyanin by spectropolarimetric titration, *Biochim. Biophys. Acta 371*, 408−416.
11. Sakurai, T., Okamoto, H., Kawahara, K., and Nakahara, A. (1982) Some properties of a blue copper protein plantacyanin from cucumber peel, *FEBS Lett. 147*, 220−224.
12. Nersissian, A. M., and Nalbandyan, R. M. (1988) Studies on plantacyanin. III. Structural data by CD and MCD methods and antigenic properties of the protein, *Biochim. Biophys. Acta 957*, 446−453.
13. Sakurai, T., Ikeda, O., and Suzuki, S. (1990) Direct electrochemistry of the blue copper proteins pseudoazurin, plantacyanin and stellacyanin, *Inorg. Chem. 29*, 4715−4718.
14. Fernández, C. O., Sannazzaro, A. I., and Vila, A. J. (1997) Alkaline transition of *Rhus vernicifera* stellacyanin, an unusual blue copper protein, *Biochemistry 36*, 10566−10570.
15. Maritano, S., Marchesini, A., and Suzuki, S. (1997) Spectroscopic characterization of native and Co(II)-substituted zucchini mavicyanin, *J. Biol. Inorg. Chem. 2*, 177−181.
16. Battistuzzi, G., Borsari, M., Loschi, L., Ranieri, A., Sola, M., Mondoví, B., and Marchesini, A. (2001) Redox properties and acid−base equilibria of zucchini mavicyanin, *J. Inorg. Biochem. 83*, 223−227.
17. Dennison, C., and Lawler, A. T. (2001) Investigations of the alkaline and acid transitions of umecyanin, a stellacyanin from horseradish roots, *Biochemistry 40*, 3158−3166.
18. Dennison, C., Harrison, M. D., and Lawler, A. T. (2003) Alkaline transition of phytocyanins: A comparison of stellacyanin and umecyanin, *Biochem. J. 371*, 377−383.
19. Harrison, M. D., and Dennison, C. (2004) Characterisation of *Arabidopsis thaliana* stellacyanin: A comparison with umecyanin, *Proteins 55*, 426−435.
20. Nersissian, A. M., Immoos, C., Hill, M. G., Hart, P. J., Williams, G., Herrmann, R. G., and Valentine, J. S. (1998) Uclacyanins, stellacyanins, and plantacyanins are distinct subfamilies of phytocyanins: Plant-specific mononuclear blue copper proteins, *Protein Sci. 7*, 1915−1929.
21. Nersissian, A. M., Hart, P. J., and Valentine, J. S. (2001) Stellacyanin, a member of the phytocyanin family of plant proteins, in *Handbook of Metalloproteins* (Messerschmidt, A., Huber, R., Poulos, T., and Weighardt, K., Eds.) pp 1219−1234, John Wiley and Sons, Chichester.
22. Nersissian, A. M., and Shipp, E. L. (2002) Blue copper-binding domains, *Adv. Protein Chem. 60*, 271−340.
23. Adman, E. T. (1991) Copper protein structures, *Adv. Protein Chem. 42*, 145−197.
24. Hart, P. J., Nersissian, A. M., Herrmann, R. G., Nalbandyan, R. M., Valentine, J. S., and Eisenberg, D. (1996) A missing link in cupredoxins: Crystal structure of cucumber stellacyanin at 1.6 Å resolution, *Protein Sci. 5*, 2175−2183.
25. Dennison, C., and Harrison, M. D. (2004) The active-site structure of umecyanin, the stellacyanin from horseradish roots, *J. Am. Chem. Soc. 126*, 2481−2489.
26. Guss, J. M., Merritt, E. A., Phizackerley, R. P., and Freeman, H. C. (1996) The structure of a phytocyanin, the basic blue protein from cucumber, refined at 1.8 Å resolution, *J. Mol. Biol. 262*, 686−705.
27. Einsle, O., Mehrabian, Z., Nalbandyan, R., and Messerschmidt, A. (2000) Crystal structure of plantacyanin, a basic blue cupredoxin from spinach, *J. Biol. Inorg. Chem. 5*, 666−672.
28. Thompson, J. D., Higgins, D. G., and Gibson, T. J. (1994) ClustalW—Improving the sensitivity of progressive multiple sequence alignment through sequence weighting, position-specific gap penalties and weight matrix choice, *Nucleic Acids Res. 22*, 4673−4680.
29. Van Driessche, G., Dennison, C., Sykes, A. G., and Van Beeuman, J. (1995) Heterogeneity of the covalent structure of the blue copper protein umecyanin from horseradish roots, *Protein Sci. 4*, 209−227.
30. Van Gysel, A., Van Montagu, M., and Inzé, D. (1993) A negatively light-regulated gene from *Arabidopsis thaliana* encodes a protein showing high similarity to blue copper-binding proteins, *Gene 136*, 79−85.
31. Mann, K., Schäfer, W., Thoenes, U., Messerschmidt, A., Mehrabian, Z., and Nalbandyan, R. (1992) The amino acid sequence of a type I copper protein with an unusual serine- and hydroxyproline-rich C-terminal domain isolated from cucumber peelings, *FEBS Lett. 314*, 220−223.
32. Bergman, C., Gandvik, E. K., Nyman, P. O., and Strid, L. (1977) The amino acid sequence of stellacyanin from lacquer tree, *Biochem. Biophys. Res. Commun. 77*, 1052−1059.
33. Schininá, M. E., Maritano, S., Barra, D., Mondoví, B., and Marchesini, A. (1996) Mavicyanin, a stellacyanin-like protein from zucchini peelings: Primary structure and comparison with other cupredoxins, *Biochim. Biophys. Acta 1297*, 28−32.
34. Murata, M., Begg, G. S., Lambrou, F., Leslie, B., Simpson, R. J., Freeman, H. C., and Morgan, F. J. (1982) Amino acid sequence of a basic blue protein from cucumber seedlings, *Proc. Natl. Acad. Sci. U.S.A. 79*, 6434−6437.
35. Mann, K., Eckerskorn, C., Mehrabian, Z., and Nalbandyan, R. M. (1996) The amino acid sequence of the spinach basic cupredoxin plantacyanin, *Biochem. Mol. Biol. Int. 40*, 881−887.
36. Solomon, E. I., Szilagyi, R. K., DeBeer George, S., and Basumallick, L. (2004) Electronic structures of metal sites in proteins and models: Contributions to function in blue copper proteins, *Chem. Rev. 104*, 419−458.
37. Thomann, H., Bernardo, M., Baldwin, M. J., Lowery, M. D., and Solomon, E. I. (1991) Pulsed ENDOR study of the native and high pH perturbed forms of the blue copper site in stellacyanin, *J. Am. Chem. Soc. 113*, 5911−5913.
38. Fields, B. A., Guss, J. M., and Freeman, H. C. (1991) Three-dimensional model for stellacyanin, a blue copper protein, *J. Mol. Biol. 222*, 1053−1065.
39. Romero, A., Hoitink, C. W. G., Nar, H., Huber, R., Messerschmidt, A., and Canters, G. W. (1993) X-ray analysis and spectroscopic

characterization of M121Q azurin. A copper site model of stellacyanin, *J. Mol. Biol. 229*, 1007−1021.
40. Dennison, C., Van Driessche, G., Van Beeumen, J., McFarlane, W., and Sykes, A. G. (1996) Electron-transfer properties and active-site structure of the type 1 (blue) copper protein umecyanin, *Chem. Eur. J. 2*, 104−109.
41. De Kerpel, J. O. A., Pierloot, K., Ryde, U., and Roos, B. O. (1998) Theoretical study of the structure and spectroscopic properties of stellacyanin, *J. Phys. Chem. 102*, 4638−4647.
42. van de Kamp, M., Canters, G. W., Andrew, C. R., Sanders-Loehr, J., Bender, C. J., and Peisach, J. (1993) Effect of lysine ionization on the structure and electrochemical behaviour of the Met44→Lys mutant of the blue-copper protein azurin from *Pseudomonas aeruginosa*, *Eur. J. Biochem. 218*, 229−238.
43. Harrison, M. D., and Dennison, C. (2004) An axial ligand at a type 1 copper site is preferable for fast electron transfer, *ChemBioChem 5*, 1579−1581.
44. DeBeer George, S., Basumallick, L., Szilagyi, R. K., Randall, D. W., Hill, M. G., Nersissian, A. M., Valentine, J. S., Hedman, B., Hodgson, K. O., and Solomon, E. I. (2003) Spectroscopic investigations of stellacyanin mutants: Axial ligand interactions at the blue copper site, *J. Am. Chem. Soc. 125*, 11314−11328.
45. Bertini, I., Fernández, C. O., Karlsson, B. G., Leckner, J., Luchinat, C., Malmström, B. G., Nersissian, A. M., Pierattelli, R., Shipp, E., Valentine, J. S., and Vila, A. J. (2000) Structural information through NMR hyperfine shifts in blue copper proteins, *J. Am. Chem. Soc. 122*, 3701−3707.
46. Koch, M., Velarde, M., Harrison, M. D., Echt, S., Fischer, M., Messerschmidt, A., and Dennison, C. (2005) Crystal structures of oxidized and reduced stellacyanin from horseradish roots, *J. Am. Chem. Soc. 127*, 158−166.
47. Sigel, H., and Martin, R. B. (1982) Coordinating properties of the amide bond. Stability and structure of metal ion complexes of peptides and related ligands, *Chem. Rev. 82*, 385−426.
48. Battistuzzi, G., Borsari, M., Menabue, L., Saladini, M., and Sola, M. (1996) Amide group coordination to the Pb^{2+} ion, *Inorg. Chem. 35*, 4239−4247.
49. Kraulis, P. J. (1991) MOLSCRIPT−A program to produce both detailed and schematic plots of protein structures, *J. Appl. Crystallogr. 24*, 946−950.
50. Creighton, T. E. (1993) *Proteins, structures and molecular properties*, 2nd ed., p 6, W. H. Freeman, New York.
51. Weber, O. A. (1974) Stability of proton and Cu(II) complexes of some tyrosine and tryptophan derivatives, *J. Inorg. Nucl. Chem. 36*, 1341−1347.
52. Nersissian, A. M., Babayan, M. A., Sarkissian, L. K., Sarukhanian, E. G., and Nalbandyan, R. M. (1985) Studies on plantacyanin. II. NMR data, redox properties, reaction with nitrite and the formation of complex with plastocyanin, *Biochim. Biophys. Acta 830*, 195−205.
53. Ullmann, G. M., Noodleman, L., and Case, D. A. (2002) Density functional calculation of pK_a values and redox potentials in the bovine Rieske iron−sulfur protein, *J. Biol. Inorg. Chem. 7*, 632−639.
54. Nunzi, F., Guerlesquin, F., Shepard, W., Guigliarelli, B., and Bruschi, M. (1994) Active site geometry in the high oxido-reduction potential rusticyanin from *Thiobacillus ferrooxidans*, *Biochem. Biophys. Res. Commun. 203*, 1655−1662.
55. Giudici-Orticoni, M. T., Guerlesquin, F., Bruschi, M., and Nitschke, W. (1999) Interaction-induced redox switch in the electron-transfer complex rusticyanin-cytochrome c_4, *J. Biol. Chem. 274*, 30365−30369.
56. Abergel, C., Nitschke, W., Malarte, G., Bruschi, M., Claverie, J. M., Giudici-Orticoni, M. T. (2003) The structure of *Acidithiobacillus ferrooxidans* c_4-cytochrome: A model for complex-induced electron-transfer tuning, *Structure 11*, 547−555.
57. Sato, K., Kohzuma, T., and Dennison, C. (2003) Active site structure and electron-transfer reactivity of plastocyanins, *J. Am. Chem. Soc. 125*, 2101−2112.

BI048256V